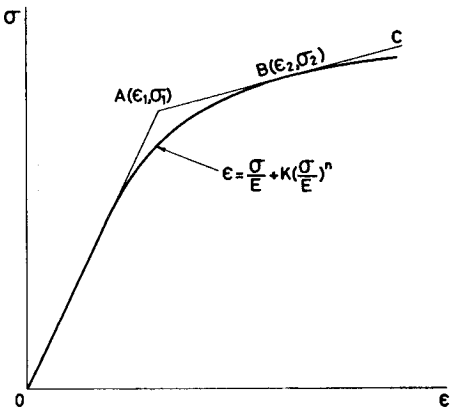

Fig. 4 The lowest modulus.

Combining Eqs. (2, 18, and 19) yields finally

$$\frac{P}{P_{cr}} = \frac{\theta_1 - \theta_o}{\theta} + \frac{1-(\theta_1/\theta)}{1+NnK(\theta_1-\theta_o)^{n-1}} \qquad \theta \geqq \theta_1 \tag{20}$$

Equations (17) and (20) describe the behavior of a material which is stiffer than the true material. Hence the curve P/P_{cr} vs θ obtained from these equations is an upper bound for the real curve.

Regarding θ_1 (point A in Fig. 4) as a floating parameter and changing it in small steps, a sequence of curves is obtained. Numerical results for two materials are shown in Figs. 2 and 3. Also, the exact results obtained before are shown.

The envelope formed by the family of the curves given by Eq. (20) can be found in the usual way. Equation (20) is rewritten in the form

$$F(P,\theta,\theta_1) = (P/P_{cr})[1+NnK(\theta_1-\theta_o)^{n-1}]\theta - NnK(\theta_1-\theta_o)^n - \theta + \theta_o = 0 \tag{21}$$

The envelope is obtained[3] by considering, simultaneously, Eq. (21) and the equation

$$\frac{\partial F}{\partial \theta_1} = \frac{P}{P_{cr}} Nn(n-1)K(\theta_1-\theta_o)^{n-2}\theta - Nn^2K(\theta_1-\theta_o)^{n-1} = 0 \tag{22}$$

or

$$\theta_1 - \theta_o = [(n-1)/n](P/P_{cr})\theta \tag{23}$$

Substitution of Eq. (23) into Eq. (21) yields the exact solution, Eq. (3). Thus, the envelope of the approximate solutions, Eq. (20), is the true behavior of the model.

The maximum load carrying capacity (for the given model) of the approximated system can be obtained as follows: differentiating Eq. (20) yields

$$\frac{d}{d\theta}\left(\frac{P}{P_{cr}}\right) = \frac{1}{\theta^2} \cdot \frac{\theta_o - NnK(\theta_1-\theta_o)^n}{1+NnK(\theta_1-\theta_o)^{n-1}} \tag{24}$$

Thus, the load increment in the second segment given by Eq. (20) is positive or negative according to the sign of the numerator in Eq. (24). Equating Eq. (24) to zero, the point $\theta_1 = \theta_1{}^{**}$, where there is no load increment from Eq. (20), is obtained

$$\theta_o - NnK(\theta_1{}^{**} - \theta_o)^n = 0 \tag{25}$$

The solution of Eq. (25) is

$$\theta_1{}^{**} = \theta_o + [(n-1)/n][\theta_o/(n-1)K]^{1/n} \tag{26}$$

and note that [see Eq. (9)]

$$\theta_1{}^{**} = [(n-1)/n]\theta^* \tag{27}$$

The maximum load for the approximate system, P^{**}, is obtained by substituting Eq. (26) into Eq. (20)

$$\frac{P^{**}}{P_{cr}} = 1 \Big/ \left[1 + nK^{1/n}\left(\frac{\theta_o}{n-1}\right)^{(n-1)/n}\right] \tag{28}$$

which is, of course, the same as the exact solution Eq. (8).

Finally it should be pointed out that the "lowest modulus" $E_L{}^{**}$ corresponding to P^{**}, is equal to the tangent modulus $E_t{}^*$ which corresponds to P^*, and that the following relations hold

$$E_t{}^*/E = P^*/P_{cr} = P^{**}/P_{cr} = E_L{}^{**}/E \tag{29}$$

Conclusions

It has been shown that, for the simple model considered, the envelope of the floating piecewise linear approximation represents the exact nonlinear solution.

References

[1] Drucker, D. C. and Onat, E. T., "On the Concept of Stability of Inelastic Systems," *Journal of the Aerospace Sciences*, Vol. 21, 1954, pp. 543–548, 565.

[2] Ramberg, W. and Osgood, W. R., "Description of Stress-Strain Curves by Three Parameters," TN 902, 1943, NACA.

[3] Courant, R., *Differential and Integral Calculus*, Vol. II, Blackie and Son Ltd., London, 1936, pp. 171–179.

Measurements in the Near Field of Supersonic Nozzles for Chemical Laser Systems

D. L. WHITFIELD,* J. W. L. LEWIS,†

AND

W. D. WILLIAMS‡

ARO Inc., Arnold Air Force Station, Tenn.

Introduction

As a contribution to the design of laser systems involving banks of multiple nozzles, the flowfields and gas mixing characteristics near the exits of two Direct Combustion Laser (DCL) nozzle banks were investigated using simulated exhaust gases.[1] The experimental techniques used in the investigation were: 1) laser Doppler velocimeter to measure flow velocities, 2) probes to measure pitot pressure, 3) electron beam to measure both relative and absolute specie number densities, and 4) electron beam to make flow visualization photographs. Also, an analytical investigation was conducted of the flow inside the nozzles, and these results were in good agreement with the experimental data.[1] Only selected results for one nozzle bank are presented in this Note.

DCL Nozzle Banks

The DCL nozzle banks were supplied by the Air Force Rocket Propulsion Lab. The nozzle bank corresponding to the present data was made of nickel. It had conical nozzles with exit diameters (d_e) of 0.234 in., area ratios of 16.85, 10° divergent wall half angles, and 0.024-in.-diam H_2 orifices. A schematic is given in Fig. 1 of the locations of four profiles for which measurements

Received July 12, 1973; presented as Paper 73-642 at the AIAA 6th Fluid and Plasma Dynamics Conference, Palm Springs, Calif., July 16–18, 1973; revision received December 26, 1973. This work was sponsored by the Air Force Rocket Propulsion Laboratory (AFRPL), Air Force Systems Command (AFSC), and the Air Force Weapons Laboratory (AFWL), AFSC. The results were obtained by ARO Inc., contract operator of the Arnold Engineering Development Center (AEDC), AFSC, Arnold Air Force Station, Tenn.

Index categories: Jets, Wakes, and Viscid-Inviscid Flow Interactions; Nozzle and Channel Flow; Lasers.

* Research Engineer, 16-P Section, Propulsion Wind-Tunnel Facility. Member AIAA.

† Senior Scientist, Aerospace Projects Branch, von Kármán Gas Dynamics Facility.

‡ Research Engineer, Aerospace Projects Branch, von Kármán Gas Dynamics Facility.

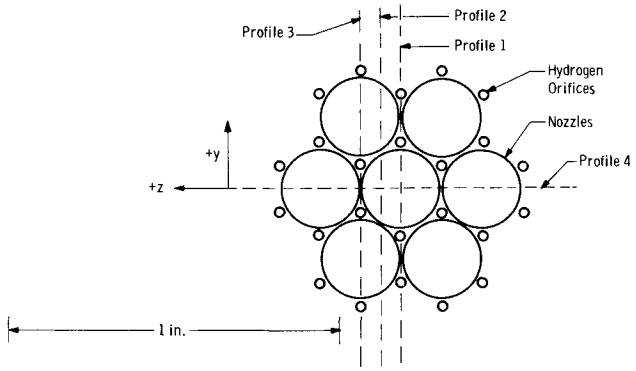

Fig. 1 Profile locations for the nozzle bank.

were made. Measurements were made at axial distances (x) of $x/d_e = 1$, 2, and 3, and as close as practical to the nozzle exit plane. The H_2 injection orifices shown in Fig. 1 were located at the nozzle exit plane.

Flow Simulation

Nozzle operating conditions were designed for the purpose of simulating the flow in the near field of the actual DCL laser nozzle banks. The following parameters were assumed to be of importance for simulation: 1) the ratio of specific heats, γ, of the gas or gas mixture through the nozzles, 2) the reservoir ratio of the number density of the diluent gas helium (He) to that of F_2 (for which nitrogen, N_2, was used in these experiments), 3) the ratio of the flow rate of the H_2 injected at the nozzle exits to the flow rate through the nozzles, 4) the ratio of the test section pressure to the total pressure of the gas through the nozzles, p_B/p_o, and 5) the viscous effects in the nozzles.[2,3] These simulation conditions were approximated by the substitution of N_2 for F_2. The nozzle operating conditions were determined as indicated in Ref. 1. For the He diluent runs, the amount of He used was $\dot{m}_{He}/(\dot{m}_{N_2} + \dot{m}_{He}) = 0.655$. The amount of H_2 injected was equal to 20% of the total mass flow rate through the nozzles. The experimental data reported in this Note were acquired for the N_2-He reservoir conditions $p_o = 219$ torr, T_o (total temperature) = 300°K, and Re_{o,r^*} (reservoir Reynolds number) = 3070.

Experimental Results

Although the velocities measured using the velocimeter were within 2% of those calculated from pitot pressure data taken in isentropic flow at high p_o, the velocimeter was of limited use because of particle lag. No gas densities of interest were high enough for the particles (the speed of which the velocimeter measures) in the gas to be accelerated or decelerated, over small distances, to the gas velocity in the shock or mixing regions.[1,4]

Pitot pressure surveys were made to determine shock locations, plume boundaries, Mach disk and jet closure locations, flow uniformity, mixing regions, and nozzle viscous effects. Pitot probe viscous effects were considered and found to be less than 2%. Numerous pitot pressure surveys are included in Ref. 1. A pitot profile at $x/d_e = 0.13$ is presented in Fig. 2. With reference

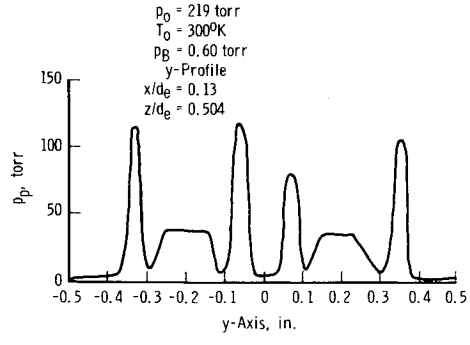

Fig. 2 Pitot pressure Profile 3 of nozzle bank at $x/d_e = 0.13$.

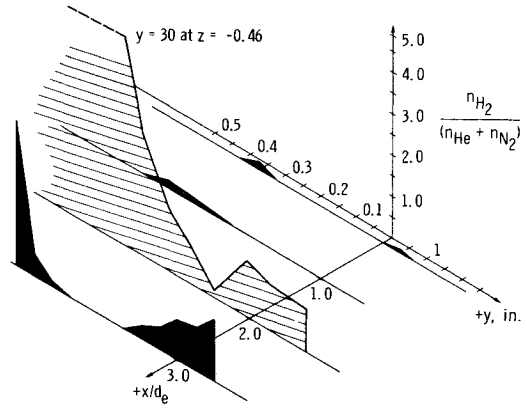

Fig. 3 Axial distance variation of density ratio for Profile 3 of nozzle bank.

to Profile 3 in Fig. 1, it is clear that the four sharp pitot pressure peaks in Fig. 2 were due to the H_2 from the injection orifices, and that the nozzle centerlines were located at about $y = \pm 0.2$ in. Specific flow features are difficult to distinguish from pitot profiles for $x/d_e > \frac{1}{2}$ and pitot probe measurements are not sufficient to resolve the question of mixing downstream of the nozzle bank.

The electron beam fluorescence technique was used to obtain flow visualization color photographs[1] and spatially-resolved specie number densities. The photographic information clearly showed the existence and location of shocks within the flowfield as well as the interaction of the nozzle and orifice flows. For quantitative estimates of the specie number densities, electron beam-excited fluorescent intensities from the He 4^1D state at 4922 Å, the $N_2^+(0, 0)$ band of the First Negative System at 3914 Å and the atomic hydrogen H_β line at 4861 Å were used. Initially optical filters were used for spectral isolation of these radiative transitions as well as the 5016 Å line from He 3^1P and the 4634 Å band of H_2, both of which were included for the purpose of redundancy in the measurement. Because of the low intensity of the H_2 band and apparently atomic nitrogen contamination radiation at 5016 Å, the two last-mentioned systems were not used in the analysis. Furthermore, a strong background continuum radiation was found to exist in the spectral vicinity of the H_β line, and resort was made to a spectrometer with photon-counting for detection of the atomic hydrogen line. The binary quenching constants required for correction of the measurements for collisional effects were either measured or estimated.[5] All relevant cross sections and methods of data reduction are presented in Ref. 5.

Following in situ calibrations, measurements of the H_2, N_2, and He absolute number densities were performed. The axial variations of the densities were measured for Profiles 1–4 shown in Fig. 1. Figure 3 shows the x and y variations of the parameter $n_{H_2}/(n_{He} + n_{N_2})$ for Profile 3. It should be noted that, if now X is the local mole fraction of H_2, the ordinate of Fig. 3 equals $X/(1-X)$. It is obvious that little penetration by H_2 of the main nozzle flow occurs before $x/d_e = 2.0$. Similar displays of the results for the other profiles are given in Ref. 1. The inaccuracy of the data of Fig. 3 is estimated to be ±25%, exclusive of spatial resolution considerations.

Summary and Conclusions

The gasdynamics in the near field of simulated chemical laser nozzle banks has been investigated experimentally by pitot pressure measurements, electron beam density measurements, and electron beam flow visualization photographs. Electron beam specie number density measurements indicated that there existed definite "H_2 layers" in the near field and complete mixing was not obtained. Although simulation of the flowfield chemistry was not attempted, the lasing characteristics are dependent upon the reactant concentrations. Consequently, it is

suggested that the gas mixing results presented in this Note represent necessary but not sufficient conditions for lasing.

References

[1] Whitfield, D. L., Lewis, J. W. L., Williams, W. D., and Mayne, A. W., Jr., "Specie Number Density, Pitot Pressure, and Flow Visualization in the Near Field of Two Supersonic Nozzle Banks Used for Chemical Laser Systems," AEDC-TR-73-11, May 1973, Arnold Engineering Development Center, Arnold Air Force Station, Tenn.

[2] Whitfield, D. L., "Theoretical and Experimental Investigation of Boundary Layers in Low Density Hypersonic Axisymmetric Nozzles," AEDC-TR-68-193, Sept. 1968, Arnold Engineering Development Center, Arnold Air Force Station, Tenn.

[3] Whitfield, D. L., "Viscous Effects in Low Density Nozzle Flows," AEDC-TR-73-52, May 1973, Arnold Engineering Development Center, Arnold Air Force Station, Tenn.

[4] Whitfield, D. L., "Dynamics of Particles in Free Molecular Flow with Application to High Altitude Meteoric Dust Collection Devices," AEDC-TR-70-139, Aug. 1970, Arnold Engineering Development Center, Arnold Air Force Station, Tenn.

[5] Lewis, J. W. L. and Williams, W. D., "Electron Beam Fluorescence Diagnostics of a Ternary Gas Mixture," AEDC-TR-73-96, July 1973, Arnold Engineering Development Center, Arnold Air Force Station, Tenn.

Buckling Behavior of a Composite Beam Column

RONALD L. MANN*
General Electric Co., Syracuse, N.Y.
AND
RICHARD W. PERKINS†
Syracuse University, Syracuse, N.Y.

AN analytical procedure was developed to predict the load vs deformation response of an axially loaded composite structure consisting of a column supported laterally by a beam. The analytical procedure was compared with an experiment which demonstrated the validity of the analysis and the existence of an interesting buckling phenomenon.

The composite beam-column system provides a means of controlling large deformations which occur when the critical load of a column is slightly exceeded. The load-deflection characteristic of a composite beam-column system would somewhat resemble that of a material tested in tension or compression rather than the characteristic column buckling curve. Thus, the composite structure system when subjected to axial loading, effectively exhibits a yield point and an ultimate strength as would a ductile material loaded beyond the elastic region.

There are a number of advantages for using the two-stage beam-column system as a structural element. Columns can be designed with a factor of safety based on a pseudo yield point, the point of first-stage buckling. For such columns used in structures, first-stage buckling would be a positive method of indicating that allowable external load levels have been exceeded. In addition, once the first-stage occurs, the remaining load carrying capacity would be known with assurance.

The beam-column system has been applied as a structural element in a design, where in addition to axial load carrying capability, elongation under solar radiation was required to be a minimum. For this application, the beam component which provided lateral support to the column absorbed the thermal energy and expanded, whereas the column shaded by the beam experienced the required minimum elongation.

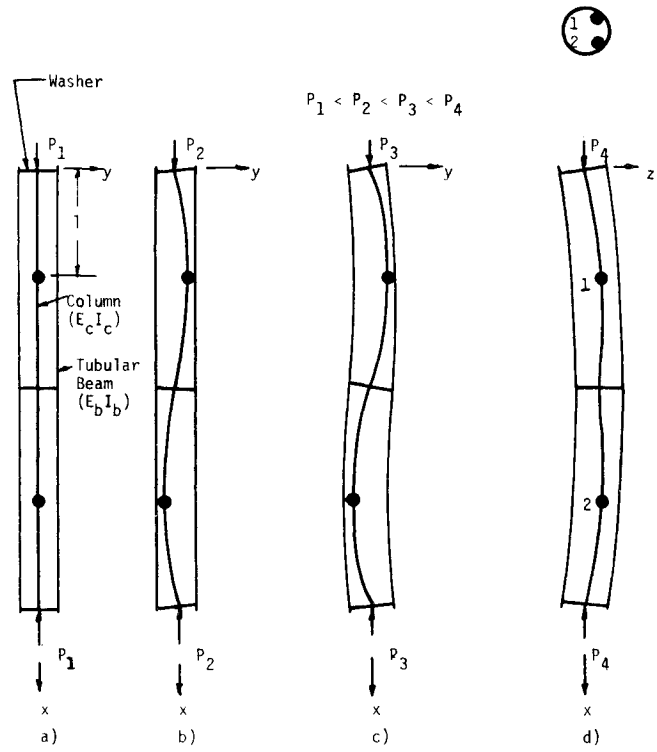

Fig. 1 Two-stage buckling of beam-column system.

The beam-column system of Fig. 1a is such that the column will buckle in the second mode with a node at the midsupport point of the beam. The beam and column parameters are selected such that the beam remains straight until the first and third quarter points of the column make contact with the beam. The beam will begin to deflect in an antisymmetrical S-shape as the axial loading continues to increase, as shown in Fig. 1c.

The general solution for determining load vs end shortening for the composite structure was based on large deflection theory for the column and small deflection theory for the supporting beam. The system was assumed to remain in the xy-plane throughout the loading process. Figure 2 shows the load deflection relationships of the column from the time that the column buckles in the first mode. P_1 is the critical first-stage buckling load given by

$$\pi^2 E_c I_c / l^2 \tag{1}$$

P_2 is the load required such that the column deflects through a distance y_1, where y_1 is the clearance between the beam and column at the first and third quarter points. The differential equation of the deflection curve for $P_1 \leqq P \leqq P_2$ is

$$E_c I_c (d\theta/ds) = -Py \tag{2}$$

for $(0 < y(l) \leqq y_1)$. For values of $P > P_2$ the differential equation is

$$E_c I_c (d\theta/ds) + Py - Hx = 0 \tag{3}$$

For a beam-column system with a given y_1, P_2 and l_2 can be found. Then setting a value of δ enables H to be determined. The general solution of the differential equation, which is similar to that given by Saelman,[1] can then be used to find an l_s and P consistent with $y(l) = y_1 + \delta$.

Assuming small deflections of the beam, H is given by

$$H = 3E_b I_b \delta / l_s^3 \tag{4}$$

where l_s is the shortened length of the beam, and δ is the beam deflection.

Received July 26, 1973.
Index categories: Structural Composite Materials (Including Loadings); Structural Static Analysis.

* Senior Engineer, Heavy Military Electronics Systems Department.
† Associate Professor, Department of Mechanical and Aerospace Engineering.